Please cite this article in press as: Abbas et al., Lipopolysaccharide nanoparticles: A biomimetic platform to study bacterial surface, Biophysical Journal (2025), https://doi.org/10.1016/j.bpj.2025.06.036

Biophysical Journal
Article

Biophysical Society

Lipopolysaccharide nanoparticles: A biomimetic platform to study bacterial surface

Massilia Abbas,[1] Samantha Micciulla,[2] Jean-Marie Teulon,[1] Meriem Maalej,[1,3] Macha Trembley,[1] Roberta Marchetti,[3] Antonio Molinaro,[3] Michel Thépaut,[1] Franck Fieschi,[1,4] Jean-Luc Pellequer,[1] and Cédric Laguri[1,*]

[1]University Grenoble Alpes, CNRS, CEA, Institut de Biologie Structurale, 38000 Grenoble, France; [2]Institut Laue-Langevin, Grenoble, France; [3]Department of Chemical Sciences, University of Napoli Federico II, Napoli, Italy; and [4]Institut Universitaire de France (IUF), Paris, France

ABSTRACT Lipopolysaccharides (LPSs) are essential components of the outer membranes of gram-negative bacteria, playing a crucial role in antimicrobial resistance, virulence, and the host's immune response. Self-assembled particles displaying LPSs are essential for biophysical studies addressing the behavior of bacterial surfaces under specific biomimetic conditions. Styrene-maleic acid copolymers were employed to form LPS nanoparticles, either from extracted LPS or directly from purified outer membranes. These nanoparticles, derived from pathogenic O157:H7 or laboratory *Escherichia coli* strains, are well-defined in size and yield high-resolution nuclear magnetic resonance spectra. They have been successfully used to investigate molecular recognition by a human C-type lectin receptor of the immune system and interaction with polymyxin antibiotics using various biophysical methods. This study highlights the significance of LPS nanoparticles as bacterial surface mimetics and opens promising avenues for further research into LPS structure and interactions. The ability to generate well-defined LPS nanoparticles offers a powerful tool for studying the molecular mechanisms underlying bacterial pathogenesis and immune response.

SIGNIFICANCE Lipopolysaccharides (LPSs) are crucial for gram-negative bacteria's outer membranes, impacting antimicrobial resistance, virulence, and immune response. The LPS nanoparticles formed provide well-defined particles for biophysical studies. These nanoparticles, from pathogenic O157:H7 or laboratory *Escherichia coli* strains, yield high-resolution nuclear magnetic resonance (NMR) spectra and are used to study molecular recognition by human immune receptors and interactions with polymyxin antibiotics. This report underscores the usefulness of LPS nanoparticles as bacterial surface mimetics and will potentially provide valuable insights into bacterial pathogenesis and immune response mechanisms.

INTRODUCTION

The outer membrane (OM) of gram-negative bacteria is essentially built up of lipopolysaccharides (LPSs), a key glycoconjugate component of its outer leaflet (1) (Fig. 1). LPSs display chemical and structural variability depending on the bacterial species and the growth conditions. Their structure is constituted of three main parts: the lipid A, formed by N- and O-acylated di-glucosamine; the core oligosaccharide (OS), a region composed of 10–15 sugars; and the O-antigen (O-Ag), a polysaccharide that can span up to 20–30 nm. Lipid A together with core OS are the most structurally conserved parts of LPS, whereas the O-Ag is highly variable, with more than 180 different O-Ag structures referenced for *Escherichia coli* (2), for instance. Gram-negative bacteria can produce incomplete LPSs lacking the O-Ag domain, therefore only composed of OS and lipid A moieties. These are referred to as lipooligosaccharides (LOSs). As schematized in Fig. 1, the LPS structures present at the bacterial surface form a heterogeneous mixture of LOS and LPS with variable O-Ag lengths, creating a complex glycan landscape.

From the biological perspective, LPSs have a dual role: 1) they form an efficient barrier, with their lipidic part forming a highly impermeable surface against entry of small molecules, and the O-Ag assembling into a thick sugar layer and contributing to OM stiffness (3); 2) they are endotoxins, as they activate the immune system of plants, animals, and humans (4). The study of LPSs remains challenging due to their

Submitted April 11, 2025, and accepted for publication June 25, 2025.

*Correspondence: cedric.laguri@ibs.fr

Samantha Micciulla's present address is Laboratoire Interdisciplinaire de Physique, UGA/CNRS UMR 5588, Grenoble, France.

Editor: Daniel Huster.

https://doi.org/10.1016/j.bpj.2025.06.036

Please cite this article in press as: Abbas et al., Lipopolysaccharide nanoparticles: A biomimetic platform to study bacterial surface, Biophysical Journal (2025), https://doi.org/10.1016/j.bpj.2025.06.036

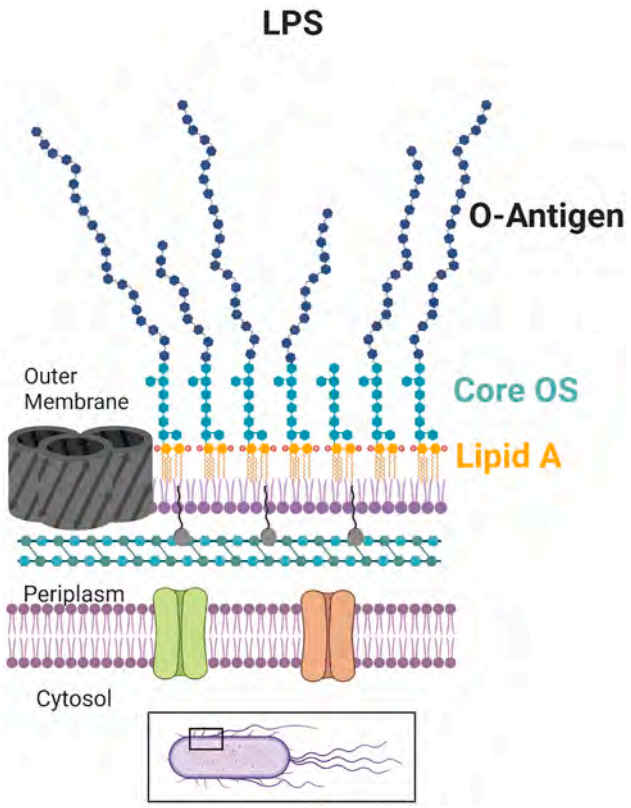

FIGURE 1 Overview of gram-negative bacteria cell envelope showing the LPS embedded into the outer leaflet of the OM. Created in https://Biorender.com.

heterogeneous and highly variable structure. LOS and LPS can be extracted from bacteria (5) but assemble into different macromolecular structures in solution depending on the size of the glycan moieties. Indeed, LOSs assemble as vesicles, whereas LPSs form tubular micellar structures (6). Given their amphiphilic nature, LPSs purification and chemical fragmentation of their different moieties is necessary for their characterization (5). However, fragmented structures lose some of their native properties, making them inadequate model systems of real bacterial surfaces. Lipid nanodiscs, also termed nanoparticles (NPs), have revolutionized the study of membrane proteins using mostly membrane scaffold proteins (7). They also hold potential applications for the reconstitution of LPS surfaces at solid and air/liquid interfaces. To generate such structures, styrene-maleic acid (SMA) copolymers have been shown to spontaneously insert into native membranes and form lipid-NPs without the prior use of detergents (8). Here, we have successfully used the SMA system to form NPs from purified LPSs and also directly from bacterial OMs of both pathogenic and model *E. coli* strains. We have demonstrated how NP-LPS can serve as biomimetic platforms, such as flat bilayers, to study LPS interactions under a variety of biologically relevant conditions, such as the interaction with a human C-type lectin receptor involved in innate immunity and antibiotics that target LPS.

MATERIALS AND METHODS

Bacterial growth

E. coli O157:H7 cells (ATCC 43888) and F653 were grown in M9 minimal medium (Na_2HPO_4 5.5 g/L KH_2PO4 3 g/L, NaCl 0.5 g/L, $MgSO_4$ 1 mM, $CaCL_2$ 0.1 mM, thiamine 2 mM), enriched with ^{15}N-NH_4Cl (1g/L) U-[^{13}C]-glucose (2 g/L) at 37°C 200 rpm until mid-exponential phase (optical density $(OD)_{260nm}$ ~1). *E. coli* F470 were grown in LB at 37°C, 200 rpm until mid-exponential phase.

SMA NPs formation and purification

E. coli F470 (R1) LOS and *E. coli O157:H7* LPS were purified using phenol/chloroform/petroleum ether and phenol/hot water methods, respectively (9,10). *E. coli R1* LOS and *O157* LPS at 1.8 mg/mL in buffer A (200 mM NaCl, 50 mM Tris pH 7.4) were incubated under gentle rocking with 1% SMA S200 (w/v) (Orbiscope) for 30 min at 25°C. Insoluble material was removed by ultracentrifugation at 100,000 × *g* for 1 h. NPs were separated from the residual SMA polymer using a sucrose gradient (prepared in buffer A) with three sucrose solutions at 45% (w/v), 25%, and 5%. Sucrose gradients were centrifuged at 100,000 × *g* overnight at 4°C. Fractions containing NPs were pooled, extensively dialyzed against buffer A, and concentrated using a vivaspin 15, with a 100 KDa cutoff.

Cells were harvested by centrifugation at 5,500× *g* at 4°C. Cells were lysed using a microfluidizer at 4°C and 15,000 psi, debris were removed by centrifugation for 20 min at 10,000× *g*, and total membrane collection by ultracentrifugation at 100,000× *g* for 1 h. Inner membranes and OMs were separated using a sucrose density gradient: 3 mL 73% (w/v), 4 mL 53% (w/v), 1 mL 20% (w/v). The OM was collected and dialyzed extensively against buffer A. The absence of inner membrane contamination was assessed by the absence of NADH dehydrogenase enzymatic activity (11). The purified OMs were solubilized using 1% SMA S200 (w/v) for 2 h at 25°C. Insoluble material was removed by ultracentrifugation at 100,000× *g* for 1 h followed by a second sucrose density gradient for residual polymer removal (45% (w/v), 25% (w/v), 5% (w/v)). The fractions containing the NPs were collected, dialyzed against buffer A, and concentrated. *E. coli F470* cells were grown in LB medium till mid-exponential phase (2.5 OD_{260nm}). OM NPs were prepared as described above. Only the sucrose gradient used for membrane separation (inner membrane and OM) was adjusted to the strain to 73% (w/v), 45% (w/v), and 20% (w/v) sucrose.

NMR

NP samples in buffer B (100 mM NaCl, 25 mM Tris pH 7.4) were lyophilized and resuspended in 100% D_2O. Around 3 mg of sample was sedimented into a 1.3-mm ssNMR rotor at 68,000 × *g* for 16 h. Spectra acquisitions were setup using ssNMRlib suite (12) for hard ^1H and ^{13}C pulse calibration as well as INEPT delays and CP parameters on a Bruker 600-MHz spectrometer equipped with MAS 1.3-mm HCN probes at 55-kHz rotation at 50°C. ^1H-detected correlation spectra were recorded using INEPT or CP transfer steps. CP transfers used typical radiofrequency-field frequencies of about 15 (^1H) and 40 kHz (^{13}C) for the H-C CP with linear ramps (50%–100%) on ^1H and a 1-ms CP length. ^1H WALTZ16 decoupling at a field strength of 10 kHz was applied in the indirect (^{13}C) dimension, whereas 15-kHz WALTZ16 decoupling was performed for ^{13}C decoupling during ^1H detection. hCH CP and hCH INEPT were typically recorded in 24–36 h. O157 O-Ag was assigned on NP-$O157_{pur}$ sample using ^{13}C (Single Quantum-J) and ^1H-detected experiments hCCH, hCH. Assignment of ^{13}C O157 LPS solubilized in detergent micelles was performed on purified O157 LPS at 4 mM in 60 mM DHPC detergent in 100% D_2O and buffer B at 50°C (^{13}C–^1H HSQC, HCCH TOCSY). All spectra were calibrated with respect to methanol (^1H 2.225 ppm ^{13}C

Please cite this article in press as: Abbas et al., Lipopolysaccharide nanoparticles: A biomimetic platform to study bacterial surface, Biophysical Journal (2025), https://doi.org/10.1016/j.bpj.2025.06.036

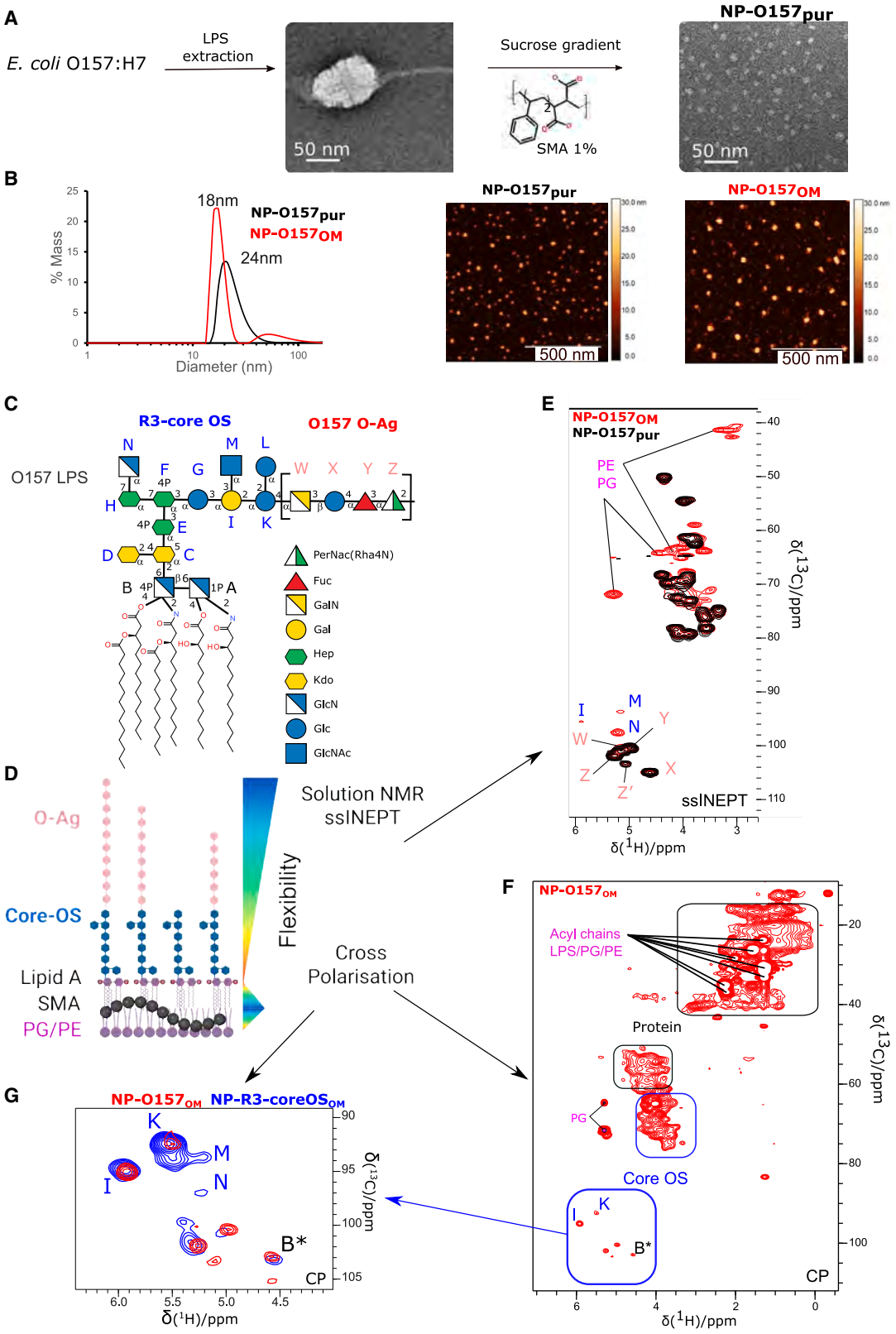

FIGURE 2 Preparation and characterization of LPS NPs. (*A*) Negative-stain electron micrographs of purified O157 LPS from the phenol phase (*left*) and after SMA solubilization showing NP-O157$_{pur}$ NPs (*right*). (*B*) Characterization of NP-O157$_{pur}$ and NP-O157$_{OM}$ by DLS (*left*) and AFM imaging (*right*). (*C*)

(legend continued on next page)

31.45 ppm), processed using TopSpin 3.5 software, and analyzed using CcpNmr analysis 2.42 software.

Biolayer interferometry

NP-R1$_{pur}$ and NP-R1$_{OM}$, in PBS buffer pH 7 (euromedex), were biotinylated nonspecifically on carboxylic groups using EDC (1-Ethyl-3-(3-dimethylaminopropyl)carbodiimide) and biotin-LC-hydrazide. From the approximate SMA concentration obtained from UV spectra at 260 nm, the EDC concentration was adjusted to react at maximum with 3% of SMA carboxylic groups. Typically for a NP sample with an OD_{260nm} of 0.2 about 15 μM EDC and 36 μM Biotin-LC-Hydrazide were incubated for 2h at 25°C, then dialyzed against PBS.

The interferometry measurements were carried out on an octet Red96 (Fortébio) using streptavidin-coated biosensors (SA). For interaction with MGL, the biotinylated NPs were immobilized in HEPES buffered saline buffer, 0.02% Tween20 to reach about 0.3 nm of response. The functionalized sensors were next equilibrated in interaction buffer (50 mM phosphate 150 mM NaCl pH 8), then immersed in the wells containing MGL at concentrations ranging from 10 to 75 nM. MGL was biotinylated on carboxyls with EDC and biotin hydrazide. Protein at 2 mg/mL in buffer (150 mM NaCl 50 mM phosphate pH 8) was treated with 1.25 mM biotin LC-hydrazide (Thermo Fisher) and 5 mM EDC for 2 h then dialyzed against the initial buffer. Proteins were immobilized at 5 μg/mL in HEPES-buffered saline buffer, 0.02% Tween20 to reach about 1 nm of response. The functionalized sensors were equilibrated in interaction buffer (50 mM phosphate 150 mM NaCl pH 8), then immersed in the wells containing R1 LOS vesicles at concentrations ranging from 0.7 to 15 μM. For interaction with polymyxins, NP-R1$_{pur}$ and NP-R1$_{OM}$ were immobilized in PBS buffer to match conditions already described (13). Immobilization level was 0.8 nm for all SA tips. All BLI data were processed and analyzed with Fortébio software after subtraction of the signal of a naked biosensor (SA) immersed in the same solution of analyte to remove the contribution of nonspecific interactions. All K_d fittings were performed with a standard 1:1 model with simultaneous fitting of all curves shown (association and dissociation).

AFM

AFM imaging was performed using a multimode 8 atomic force microscope with a Nanoscope V controller (Bruker). Imaging was performed in air using the PeakForce Tapping mode with a ScanAsyst Air cantilever (k = 0.4 N/m, Fq = 67 kHz). Images were recorded with a scan size of $2 \times 2\ \mu m^2$, at a line rate of 1 Hz and a resolution of $512 \times 512\ px^2$, using a semi-manual ScanAsyst control of the setpoint and/or gain. Data corrections include a plane leveling followed by a median line leveling using Gwyddion (14). Stripe noise has been evaluated using DeStripe (15) and visibility improvement has been tested using the Laplacian weight filter (16,17).

All samples were loaded on a freshly cleaved mica surface coated with Ni^{2+} ion as follows. First, 3-μL of $NiCl_2$ at 2 mM was incubated for 2 min followed by drying under a gentle nitrogen flow. Then, 3 μL of 30–120 μg/mL solution of NP was applied and deposited for 2 min on the Ni-coated mica surface and dried under a nitrogen flow. Individual MGL proteins were diluted to 4.7 μg/mL before deposition on Ni-coated mica. The complex of MGL (4.7 μg/mL) and NP-R1pur (34 μg/mL) was incubated for 10 min before deposition.

Height and surface area were computed with Gwyddion using a standard grain analysis with a threshold segmentation. Individual grain heights were computed by subtracting the background height from the maximum height of the segmented grains. Grains were selected using a threshold of one-third of the maximum image height, whereas the threshold for the background was the lower 10%. Grains were filtered by removing grains of smaller size (<400 nm^2 surface area), a value corresponding to the lower limit of the global average size of the smallest NPs observed in this study. Height measurements were performed using Gwyddion's "Distribution of various grain characteristics" tool, exported as text data, and further processed in Excel. Height and surface area were obtained from two different images.

MGL-ECD expression and purification

Human MGL isoform 2 extracellular domain (residues Q61-H292 Uniprot: Q8IUN9-2) with an N-terminal Strep-tag II and a factor Xa cleavage site (MASWSHPQFEKIEGRGGG) was expressed and purified as already reported after refolding (10,18).

DLS

DLS data of NPs were recorded at 25°C on Wyatt Dynapro Nanostar. For each sample, 10 acquisitions of 5 s were recorded and analyzed in percentage of mass.

QCM-D

QCM-D experiments were carried out on a Q-Sense E4 instrument from Biolin Scientific (Gothenburg, Sweden). The quartz crystals were coated with 100-nm gold substrate (model QSX 301) and fundamental resonance frequency of 4.95 MHz. Before use, the crystals were rinsed with a sequence of organic solvent (chloroform, ethanol, acetone) and water under sonication for 30 min, dried under nitrogen stream, and treated by UV-ozone for 30 min. The baseline of QCM-D measurement was measured in the same buffer used for the experiments: 25 mM Tris, 100 mM NaCl, pH 7.4 for the study of MGL binding, and 50 mM phosphate, 150 mM NaCl, pH 8 for the PmB adsorption studies. After establishing a stable baseline signal, a solution of NP-R1$_{pur}$ (0.5 mg/mL) was injected at a flow rate of 100 μL/min. The protein was injected at a concentration of 12 μM in the same buffer as for the preparation of the lipid bilayer. The same holds for the injection of PmB, which was prepared at a concentration of 70 μM, in reference to previous studies on model bacterial membranes (19). Data were collected using the Q-Soft software, provided by the company, and converted into data files with QTools.

RESULTS AND DISCUSSION

Formation and characterization of LPS NPs from pathogenic O157:H7 *E. coli*

LPS from pathogenic *E. coli* O157:H7 was first investigated to validate the formation of LPS NPs with SMA polymers on a biologically relevant system. This enterohemorrhagic strain is responsible for regular foodborne outbreaks and its O-Ag is essential for virulence (20,21). O157 LPS was first purified from bacteria using the phenol/chloroform/light petroleum method (5). When extracted from the phenol phase, it

Chemical structure of *E. coli* O157 LPS with sugars represented in standard glycan nomenclature snfg (22). (*D*) Scheme of NMR characterization of NP-O157 depending on the relative flexibility of the different parts of the system, created in https://Biorender.com. (*E*) Overlay of ssINEPT ^{1}H-^{13}C spectra of NP-O157$_{pur}$ and NP-O157$_{OM}$. (*F*) CP of NP-O157$_{OM}$ with the different component of OM components highlighted. (*G*) Comparison of core OS signals in NP-R3$_{OM}$ and NP-O157$_{OM}$. *Assessed from (23,24).

Please cite this article in press as: Abbas et al., Lipopolysaccharide nanoparticles: A biomimetic platform to study bacterial surface, Biophysical Journal (2025), https://doi.org/10.1016/j.bpj.2025.06.036

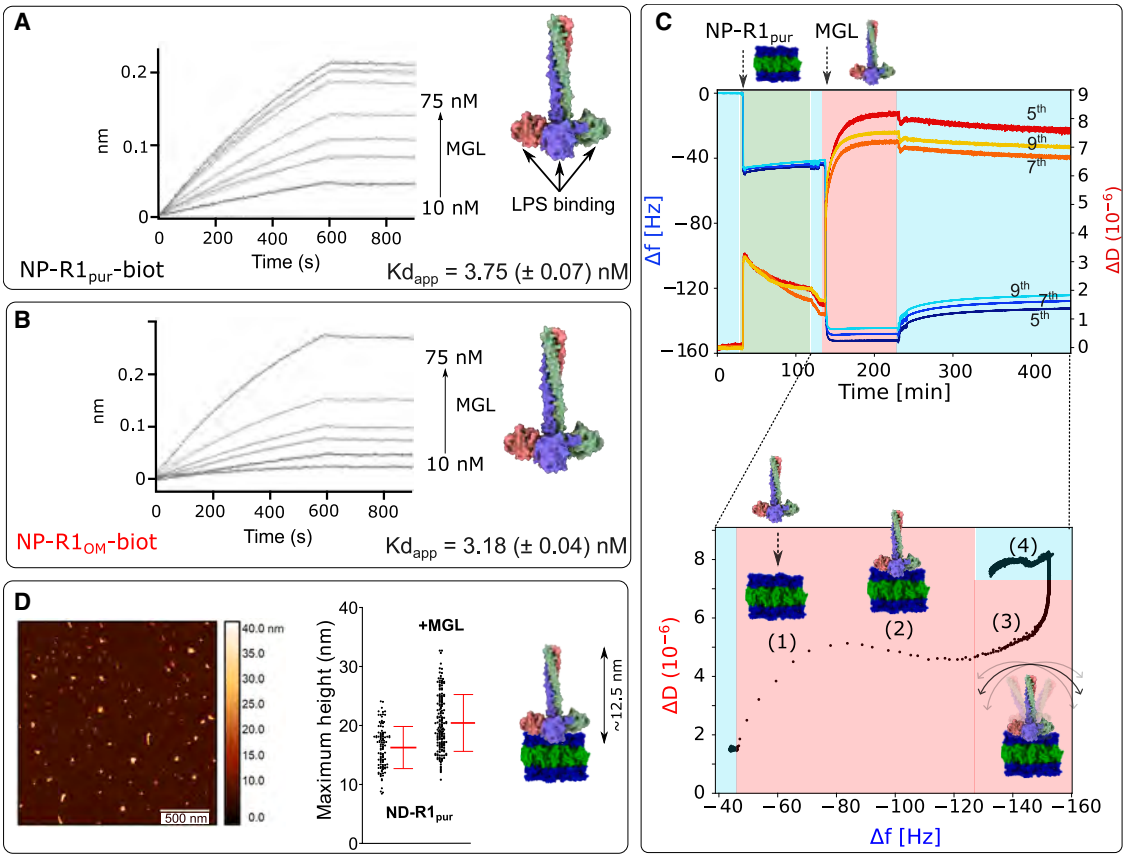

FIGURE 3 NP-R1$_{pur}$ -MGL Interaction. Biolayer interferometry interaction of immobilized NP-R1$_{pur}$-Biot (*A*) and NP-R1$_{OM}$-Biot (*B*) with increasing concentrations of MGL. MGL trimer model (10) is shown. (*C*) Top: frequency (Δf) and dissipation energy (ΔD) monitoring for the fifth, seventh, and ninth overtones during NP-R1$_{pur}$ adsorption (*green background*) and MGL binding (*red background*). The rinsing steps (*buffer*) are marked with a cyan background. Bottom: ΔD vs. Δf plot of MGL adsorption and rinsing phase with proposed schemes of structural rearrangement at the interface. (*D*) AFM imaging of NP-R1$_{pur}$ upon incubation with MGL (*left*) with corresponding heights distribution (*right*) with error bars showing mean value and standard deviation. MGL model is shown at the same scale with a symmetrical R1 LPS bilayer (lipid A (*green*), core OS (*blue*)).

assembles into large and heterogeneous membrane structures (Fig. 2 *A*). Purified O157 LPS was then incubated with SMA S200, and remaining membranes were pelleted by ultracentrifugation. The supernatant, containing NPs, was subjected to a sucrose gradient to remove free polymers (see materials and methods section) and the samples are referred to as NP-0157$_{pur}$. Negative-stain transmission electron microscopy, dynamic light scattering (DLS), and atomic force microscopy (AFM) confirmed the successful formation of NPs with a relatively homogeneous size distribution (Figs. 2 *A*, *B*, and S1).

Using a different approach, LPS NPs were formed by directly incubating purified OMs of *E. coli* O157:H7 with SMA polymers, relying on the polymer ability to extract lipids directly from the native membranes (25). In this approach, bacterial disruption was followed by the separation of outer and inner membranes via a sucrose gradient (11). Isolated OMs were then treated with SMA polymer, and the resulting NPs were isolated as described above for purified LPS. These samples are referred to as NP-0157$_{OM}$. DLS measurements showed the formation of a majority of NPs with a mean diameter of 18 nm with lower polydispersity compared to NP-O157$_{pur}$ (Fig. 2 *B*). Given the low contrast of NPs in negative-staining electron microscopy, the samples were imaged by AFM. NPs were adsorbed onto a mica surface coated with Ni^{2+} ions and imaged in air under ambient conditions. AFM images showed well-defined NPs for both NP-O157$_{OM}$ and NP-O157$_{pur}$ (Figs. 2 *B* and S1). Analysis of all particles shows a bimodal distribution for AFM, similar to that observed with DLS, with a majority of small NPs (Fig. S1, bottom) and a wide distribution of larger particles. The diameter mode of the smaller particles is approximately 8 nm for both NP-O157pur and NP-O157OM, whereas the diameter mode of the larger particles is approximately 32 and 44 nm, respectively. The formation of LPS NPs with SMA is thus effective and allows the formation of NPs of diameter about 10–50 nm.

NMR investigation of NP-O157

NMR spectroscopy is a powerful technique to study structure and interactions of LPS-containing systems. It is nondestructive and allows probing molecular structures at the

Please cite this article in press as: Abbas et al., Lipopolysaccharide nanoparticles: A biomimetic platform to study bacterial surface, Biophysical Journal (2025), https://doi.org/10.1016/j.bpj.2025.06.036

atomic scale. For this purpose, ^{13}C is necessary for a gain in sensitivity and the possibility to acquire NMR correlation experiments through ^{13}C nuclei. NPs were thus formed with LPS from bacteria grown in minimal medium with ^{13}C glucose as sole carbon source (9). NP-O157$_{pur}$ was analyzed first by solution NMR. Because of high thermal stability of SMA NPs (8), experiments could be recorded at 50°C for favorable molecular tumbling. The resulting NMR spectra show with high sensitivity the signals of the O-Ag tetrasaccharide repeat of O157 (Fig. 2 *C*), which is highly flexible (Fig. S2). In contrast, moieties closer to the membrane (lipid A and core OS) were not observable due to the slow molecular tumbling of NPs in solution. Magic angle spinning (MAS) NMR, on the other hand, enables average strong couplings that limit solution NMR of large macromolecules and has been particularly useful to study both rigid and flexible parts of complex cell wall glycoconjugates (6,23,26,27). ^{13}C-labeled NPs were sedimented inside 1.3-mm rotors and studied at 55-kHz rotation with ^{1}H-detected experiments through two types of correlation transfer, cross-polarization (CP) and insensitive nuclei enhanced by polarization transfer (INEPT). These experiments are overall sensitive to rather rigid or more mobile parts of the system, respectively (Fig. 2 *D*). NP-O157$_{pur}$ ^{13}C-^{1}H INEPT is identical to the spectrum in solution (Fig. S2) and shows the O-Ag as well as the CH_2s and CH_3 of the extremity of the lipid A acyl chains, which are still very dynamic inside the membrane (6). The O-Ag ^{1}H and ^{13}C resonances could be assigned under MAS by ^{1}H-detected and ^{13}C-detected experiments (Fig. S3).

NP-O157$_{OM}$ ^{13}C-^{1}H INEPT spectrum shows perfect superimposition of the O-Ag signals with NP-O157$_{pur}$ (Fig. 2 *E*). As expected, NP-O157$_{OM}$ shows additional signals corresponding to OM components. Phospholipid head groups from phosphatidyl-ethanolamine and phosphatidyl glycerol were also observed, as well as lipid modifications such as unsaturation of fatty acids (6). (Figs. 2 *E* and S4). ^{1}H-^{13}C CP spectra, on the other hand, tend to select rigid parts. O157 O-Ag is filtered out and the CP ^{1}H-^{13}C spectrum displays signals characteristic of proteins that were coextracted with LPS (Figs. 2 *F* and S4). Although the spectrum of OM NPs is complex due to its heterogeneous composition, the sugar anomeric resonances (H_1–C_1) were well resolved in the 90- to 105-ppm region in ^{13}C (Figs. 2 *F* and *G*). NMR assignment of these sugar resonances using CP-based experiments was unsuccessful due to low sensitivity. However, they presumably arise from the core OS and lipid A sugars. O157 core OS is of R3 type (28) (Fig. 2 *C*). Therefore, NPs from the OM of F653 *E. coli* strain, which produces LOS containing the R3 type core OS, were produced. ^{13}C-^{1}H INEPT spectrum of NP-R3$_{OM}$ is superimposable to NP-O157$_{OM}$ spectra, except for the absence of O-Ag signals (Fig. S4). The anomeric region of NP-O157$_{OM}$ and NP-R3$_{OM}$ in CP-based experiments (Fig. 2 *G*) largely overlap, confirming the signals arise from the core OS. Some of these core OSs anomeric groups could be assigned (I, M, N, K) by solution NMR of O157 LPS solubilized in detergent micelles (see materials and methods section) (Figs. 2 *G* and S5). Their chemical shifts are very similar to the assignments of R3 core OS from the literature (29). Assignment of lipid A glucosamine (B) remains tentative but corresponds to a highly substituted glucosamine with chemical shifts similar to previous reports (23,24). Overall, NMR analysis of NPs consistently shows high-resolution spectra either in solution or solid-state NMR depending on the relative flexibility of the different molecular components.

NP-LPS constitutes a relevant platform to explore interactions with a lectin from the immune system

We next investigated the potential use of NP-LPS to reconstitute bacterial surfaces for recognition studies. As a proof of concept, a simple system was chosen that contains only LOS (without O-Ag). The R1 core OS is extensively used to study interactions with proteins (10,18,30,31) and is the major core type found in pathogenic *E. coli* (28). Therefore, NP-R1$_{pur}$ and NP-R1$_{OM}$ were produced following the same approach as for O157 LPS (see materials and methods section and Fig. S6). The human macrophage galactose-type lectin (MGL) was selected as a test protein. This trimeric C-type lectin receptor, expressed in dendritic cells, binds R1 core OS on *E. coli* surface with high affinity thanks to two LPS-binding sites per MGL monomer (10). To assess this interaction, NP-R1$_{pur}$, composed only of LOS molecules, was first functionalized with a biotin through its maleic acid moieties, as previously described (32), and immobilized on streptavidin-coated biolayer interferometry (BLI) sensors (see materials and methods section). Injections of increasing concentrations of MGL show a dose-dependent interaction and a very slow dissociation. Association and dissociation kinetics could be fitted to an apparent affinity constant of 4 nM (Figs. 3 A and S7), consistent with the observation of stable binding of MGL to *E. coli* surface (10). As a control, MGL was biotinylated and immobilized on BLI biosensors. Purified R1 LOSs, which assemble spontaneously as vesicles of various sizes in solution, were flowed over immobilized MGL (Fig. S8). Similarly, dissociation was very slow and an apparent K_d of 129 nM could be determined for MGL-biot:R1 vesicles affinity, much higher than the 4 nM estimated for NP-R1pur-biot:MGL. It can be hypothesized that only a small proportion of LOSs are available for binding on the spherical vesicles. This, in turn, would highly increase the apparent K_d. Biotinylated NP-R1$_{OM}$ were also immobilized on BLI and tested for MGL interaction. A K_d of 3 nM could be estimated, demonstrating that NP-R1$_{OM}$ can also be used to assess protein binding to LPS.

These results demonstrate that LOS NPs are valuable platforms to assess the kinetics of protein-LPS interactions

Please cite this article in press as: Abbas et al., Lipopolysaccharide nanoparticles: A biomimetic platform to study bacterial surface, Biophysical Journal (2025), https://doi.org/10.1016/j.bpj.2025.06.036

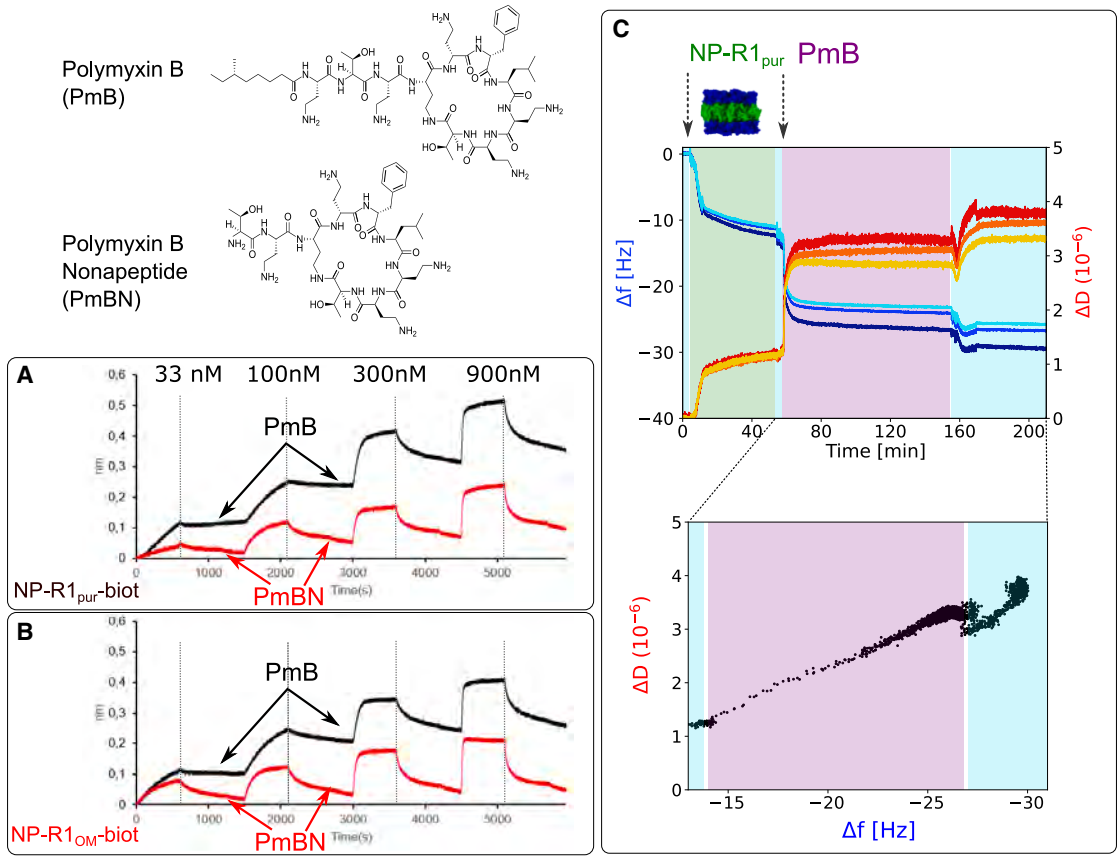

FIGURE 4 Interaction of NP-R1$_{pur}$ and NP-R1$_{OM}$ with polymyxins. PmB and PmBN are allowed to associate and dissociate at increasing concentrations over immobilized NP-R1$_{pur}$ (*A*) or NP-R1$_{OM}$ (*B*). (*C*) Frequency (Δf) and dissipation energy (ΔD) monitoring for the fifth, seventh, and ninth overtones during NP-R1$_{pur}$ adsorption and PmB binding. The NP adsorption is marked with green background and the PmB adsorption with purple background. The rinsing steps (buffer) correspond to the cyan background in the plot.

by BLI. However, more accurate structural information on the protein-lipid interaction is beyond the capability of this method. For this purpose we carried out quartz crystal microbalance with dissipation monitoring (QCM-D) experiments to study the properties of NP-R1$_{pur}$ deposited onto a solid substrate and the binding of MGL. QCM-D is a highly sensitive technique to mass variation and viscoelastic properties of thin films adsorbed onto a solid surface. It exploits the piezoelectric properties of quartz to drive a crystal to its resonance frequency and higher overtones applying an alternating voltage across its surface. All the variations of these oscillation frequencies due to the coupling of a mass on the sensor surface produce a change of frequency shift (Δf), which is proportional to the coupled mass (with negative variation for added mass, and vice versa). Moreover, the instrument allows the quantification of the energy dissipated by the bound system (ΔD), whose amplitude changes according to the viscoelastic character of the adsorbed layer. This simultaneous acquisition of the Δf and ΔD at different overtones is crucial to study binding and conformational changes of biomolecular systems, which have in most cases a very pronounced frequency-dependent behavior (33). In our experiment (Fig. 3 *C*), NP-R1$_{pur}$ was deposited onto a gold-modified quartz crystal, showing a fast adsorption kinetics (green background in Fig. 3 *C*) and a very stable binding, with no significant mass loss over time. The measured frequency shift of about −40 Hz is consistent with the deposition of a lipid bilayer. The slightly higher values for both Δf and ΔD (ΔD $\sim 2 \times 10^{-6}$) compared to canonical phospholipid bilayers (Δf ~ -30 Hz, ΔD ≤ 1) (34) can be explained by the higher hydration of sugar moieties of the core OS and the presence of charged polymer units (SMA belt). Under the validity of the Sauerbrey model (35) and assuming an approximate film density of 1 mg/cm^3 (36), we obtain a thickness of 7.6 ± 0.2 nm for deposited NP-R1$_{pur}$ (37). This is in good agreement with values reported for supported lipid bilayers and the expected thickness of a pure LOS bilayer (about 8.5 nm). The injection of MGL protein (red background in Fig. 3 *C*) generated a significant negative frequency shift (Δf of ∼90 Hz), consistent with a large mass increase upon protein binding. Furthermore, the increase of dissipation energy (ΔD $\sim 7.0 \times 10^{-6}$) is a typical indication of the presence of a highly hydrated and flexible mass. In support to this interpretation, both Δf and ΔD show a constant overtone splitting upon equilibration consistent with an increase in height of the system. Finally,

Please cite this article in press as: Abbas et al., Lipopolysaccharide nanoparticles: A biomimetic platform to study bacterial surface, Biophysical Journal (2025), https://doi.org/10.1016/j.bpj.2025.06.036

the minor variations measured upon rinsing and long equilibration times showed a strong and stable interaction of MGL with R1 core OSs (Fig. 3 *C*, cyan background), consistent with the stable complexes observed in BLI.

A more accurate interpretation of the adsorption process and possible structural rearrangement at the surface could be extracted from the representation of ΔD versus Δf traces from the MGL adsorption (red) and rinsing (blue) phases (Fig. 3 *C* bottom). Four different phases of MGL behavior can be observed from ΔD versus Δf traces (1–4 Fig. 3 *C*). First, the large separation of the data points at the beginning of MGL injection (phase 1) demonstrated the strong affinity and quick binding of the protein to the NPs. This was followed by a slower filling of the surface (phase 2: Δf decrease, ΔD constant or slightly increasing). Such a slower mass adsorption process can be explained by the decrease of available binding site and their more difficult accessibility due to the steric hindrance of bound protein molecules. When the surface saturation was approached (constant Δf $\sim$150 Hz), the ΔD started increasing abruptly, which we interpret as a structural rearrangement (phase 3) of highly viscoelastic character under constant adsorbed mass. According to the protein structure, this trace could be the signature of a rotation and oscillation of its elongated, outermost region, and it might possibly involve some minor rearrangements of the underneath NPs to allow an energetically more favorable protein conformation. At the final rinsing step (phase 4), a minor mass loss was registered, most likely due to loosely bound protein molecules that are rinsed from the interface, whereas the viscoelastic character was constant, a clear indication of the MGL stability onto the NP-R1$_{pur}$ surface. Note that this specific molecular rearrangement is characteristic of MGL only when it binds onto the LPS NP. As a control experiment, we have adsorbed the same concentration of MGL onto a bare gold substrate (Fig. S9 *A*). In this case, although the adsorbed mass is comparable (Δf ~ -88 Hz), the increment of dissipation is much lower ($<2 \times 10^{-6}$) and no overtone splitting is observed. This means that a rigid mass is bound onto the substrate with MGL most probably adsorbing in a flat, horizontal conformation, in contrast to the vertically oriented conformation when it binds to the R1 surface. Accordingly, the direct ΔD versus Δf comparison showed a rather simple trend with a fast initial mass increment with low dissipation energy, a constant plateau, and a minor dissipation decrease during rinsing.

In conclusion, biolayer interferometry and QCM-D confirm a strong interaction of MGL with LOSs at the surface of NPs and, as expected from the localization of MGL sugar-binding domains, an orientation of MGL perpendicular to the NP surface. Height measurements of NP-R1$_{pur}$ in complex with MGL using AFM further supported this orientation of MGL on LPS surface. The measurements indicated an increase in the mean height of NPs of approximately 4 nm (see Figs. 3 *D* and S10). This increase is presumably attributable to MGL-carbohydrate recognition domains that are bound to the surface. Additionally, a substantial rise in the maximum height of the complexes was observed, reaching approximately 8 nm for a maximum size of MGL trimer estimated to be 12.5 nm (10) (Fig. 3 *D*). This finding aligns with the perpendicular binding of MGL on LPS, which exhibits a degree of flexibility, as shown by the viscoelasticity determined through QCM-D.

NP-LPS and antimicrobial peptide interaction

LPSs constitute the target of polymyxin antibiotics, positively charged cyclic peptides (Fig. 4), which interact with the lipid A through the phosphate moieties and divalent ions. This family of antimicrobial peptides is used mostly against multi-drug-resistant gram-negative bacteria as last-resort treatment due to its high toxicity (38). Although the exact mode of action of polymyxins is still controversial, they are able to accumulate at the OM and disrupt LPS assembly, causing cell death (39). Recent investigations of polymyxin B (PmB) and its nonlethal variant polymyxin B nonapeptide (PmBN), which lacks PmB terminal amino acid and acyl chain (Fig. 4), shed light on the PmB mechanism. PmB interacts with LPS with high affinity at low-nanomolar concentrations until the LPS surface is saturated, then binds with lower affinity with fast association and dissociation kinetics (13). On the other hand, PmBN only displays the low-affinity component of PmB interaction without accumulation in the LPS surface. This behavior observed by Buchholz and colleagues on *E. coli* cells and OM vesicles by surface plasmon resonance was investigated on NP-R1$_{pur}$ and NP-R1$_{OM}$ by BLI (Fig. 4). Consecutive injections of PmB and PmBN were performed on the same biosensors loaded with NP-R1$_{pur}$ or NP-R1$_{OM}$ to observe surface saturation. At low PmB concentrations (33 and 100 nM; Fig. 4 *A* and *B*), no dissociation is observed, consistent with accumulation of PmB at the LPS surface. Higher concentrations injected show low-affinity kinetics as the LPS surface becomes saturated with PmB. PmBN, on the other hand, does not show accumulation to the surface and only low-affinity kinetics, as previously described (13). The same kinetics were observed for LPS NPs either purified or extracted from the OM.

As for MGL binding, the interaction of PmB with the LPS layer was assessed by QCM-D. In Fig. 4 *C* we report the variation of Δf and ΔD for the adsorption of NP-R1$_{pur}$ (green background) followed by the injection of PmB (purple background). First of all, we can observe in this case a different mechanism of formation for the lipid bilayer, with slower adsorption kinetics and an overall lower adsorbed mass (Δf ~ -14 Hz). This could be explained by the different experimental conditions, more precisely the use of a different buffer (see materials and methods). Despite the different binding kinetics and total mass, the QCM-D data

Please cite this article in press as: Abbas et al., Lipopolysaccharide nanoparticles: A biomimetic platform to study bacterial surface, Biophysical Journal (2025), https://doi.org/10.1016/j.bpj.2025.06.036

confirm the stable NP binding. The injection of PmB produced an additional mass increment (Δf ~-13 Hz), accompanied by dissipation energy increment and overtone splitting. Given the small size of the peptide, the experimental overtone separation could be explained by the creation of defect in the bilayer upon insertion of PmB. This can lead to heterogeneity, and therefore more hydrated domains, or to the reorganization of the polymer belt around the NPs, whose negative charges might promote some additional interaction with the positively charged peptide. Noteworthy, the total variation of the frequency shift is in this case significantly lower than for MGL, which is reasonable considering the different structure of the two molecules. The rinsing with buffer did not produce a clear mass loss but, apparently, an additional increment of the layer hydration. The overall interpretation of LPS-PmB interaction can be further rationalized from the interpretation of the corresponding ΔD versus Δf plot. We can clearly identify the fast adsorption from the frequency and dissipation increment following the PmB injection (purple background), which varies with a comparable rate; this is followed by a stabilization of both signals. The final rinsing step leads to a minor mass and dissipation increment, which is most likely due to water entering some defects in the bilayer. The control experiment for PmB adsorbing onto a bare gold substrate (Fig. S9 *B*) shows a comparable variation of Δf (~-13 Hz) but with a much lower dissipation increment, signature of a flat, rigid layer adsorbed onto the substrate. The final rinsing of the PmB (light blue background) indicates some mass loss with a constant dissipation (Δf $\sim$9 Hz), possibly due to the removal of loosely bound molecules but leaving the surface properties unchanged. NP-LOS is thus able to report interactions with antimicrobial peptides that either interact transiently like PmBN and have poor bacterial killing ability, and PmB that, on the other hand, are able to insert into the LPS membrane and be bactericidal at low concentration.

CONCLUSIONS

Cell-surface glycoconjugates are ubiquitous and present on almost all cell surfaces, anchored to various macromolecules such as proteins or lipids. In bacteria, LPSs, lipoteichoic acids, and mycobacterial glycolipids are essential components of cellular surfaces. These molecules play both structural and functional roles in resistance to external factors and interactions with hosts. The remarkable chemical diversity of these glycoconjugates and their surface presentation create a heterogeneous three-dimensional mesh, complicating their study in vitro under conditions that mimic their natural configuration. The objective of this study was to develop a unified platform for studying LPSs of different compositions. LPS from pathogenic bacteria or LOSs from laboratory strains, purified by solvent extraction, were assembled into NPs upon incubation with SMA polymers. Similarly, simple OM purification followed by incubation with SMA also allowed NP formation. All tested LPS NPs exhibited thermal and long-term stability similar to previously reported lipid-SMA NPs. NMR studies, using ^{13}C labeling, provided atomic-scale information on individual glycolipid groups with high resolution through both solution and solid-state NMR in reasonable acquisition times. Solution and solid-state NMR have previously been successfully applied to study cell wall components (LPS, peptidoglycan, capsular polysaccharides) (6,27,40). The main advantage of LPS NPs is that the same sample can be analyzed by solution and solid-state NMR but also further explored through other biophysical methods without modifications. Peptidoglycan or LPS, for example, require enzymatic or chemical degradation to be studied by different methods. These treatments lead to a lack of some structures or modifications and a presentation of the glycoconjugate very different from their native context.

To test the suitability of these NPs, we chose the simplest and most well-characterized LOSs. We investigated the interaction of a human C-type lectin receptor with the LPS, measuring kinetics data, physicochemical behavior using QCM-D, and topography using AFM. These data are consistent with current knowledge of MGL binding to LPS on bacterial surfaces through strong multivalent adhesion, with an orientation of the protein perpendicular to the membrane (10). Additionally, we tested the interaction of LPS-assembled NPs with antimicrobial peptides, allowing us to observe nonreversible embedding into the LPS membrane.

The assembly of biologically important glycolipids into a stable platform, accessible to multiple analytical techniques, represents a significant advancement in the study of bacterial surfaces. They allow biophysical study of the LPS as well as interaction with its ligands, not only in bulk but also upon immobilization of solid substrates. Furthermore, NPs formed directly from purified OMs do not require complex extractions that vary in efficiency depending on the LPS structure and can be formed from various bacterial strains. Recently, SMA NPs from *Pseudomonas aeruginosa* OM vesicles have also been successfully used to vaccinate mice and monitor phagocytosis (41). SMA polymers are also easy to functionalize and immobilize on several supports. More than two dozen polymers capable of forming native NPs have been developed and are commercially available (https://smalp.net). This allows the nature of hydrophobic or hydrophilic moieties of the polymer to change easily. Polymer change can alter the size of NPs generated but also their susceptibility to divalent ions, the main limitation of the SMA polymers.

One of the most interesting perspectives of our study would be the use of functionalized OM NPs from various pathogenic bacteria to design specific LPS glycan arrays. This would enable us to take into account the multivalency

Please cite this article in press as: Abbas et al., Lipopolysaccharide nanoparticles: A biomimetic platform to study bacterial surface, Biophysical Journal (2025), https://doi.org/10.1016/j.bpj.2025.06.036

of the real bacterial surface to screen for ligands (proteins, antibodies, small molecules). The same NPs could be used to further explore interaction hits with biochemical and biophysical methods.

ACKNOWLEDGMENTS

We thank the Agence Nationale de la Recherche (ANR) PIA for Glyco@Alps (ANR-15-IDEX-02) for the support of M.M., the Mizutani foundation for glycosciences (no. 230030) for their support of C.L., and the Grenoble Alliance for Integrated Structural and Cell Biology (ANR-17-EURE-0003) for funding M.A. This work used platforms of the Grenoble Instruct-ERIC center (ISBG; UAR 3518 CNRS-CEA-UGA-EMBL) within the Grenoble Partnership for Structural Biology, supported by FRISBI (ANR-10-INBS-0005-02). S.M. acknowledges the Partnership for Soft Condensed Matter at the ILL for granting access to the preparation laboratories and to the instrumentation for the QCM-D experiments. C.L. was granted access to the CCRT High-Performance Computing facility under grant CCRT2023-lagurice awarded by the Fundamental Research Division (DRF) of CEA. This work acknowledges the AFM platform at the IBS. We thank B. Bersch for stimulating discussions and A. Vallet for technical help. This project has received funding from the European Research Council under the European Union's Horizon 2020 research and innovation program under grant agreement no 851356 to R.M.

AUTHOR CONTRIBUTIONS

C.L., S.M., and J.-L.P. designed the research. C.L., S.M., J.-L.P., and M.A. wrote the manuscript. C.L., S.M., J.-L.P., M.A., J.-M.T., M. Trembley, M. Thépaut, M.M., and F.F. performed the research. C.L, S.M., J.-L.P., M.A., and J.-M.T. analyzed the data.

SUPPORTING MATERIAL

Supporting material can be found online at https://doi.org/10.1016/j.bpj.2025.06.036.

REFERENCES

1. Lorenzo, F. D., K. A. Duda, …, A. Molinaro. 2021. A Journey from Structure to Function of Bacterial Lipopolysaccharides. *Chem. Rev.* 122:15767–15821.
2. Liu, B., A. Furevi, …, G. Widmalm. 2020. Structure and genetics of escherichia coli O antigens. *FEMS Microbiol. Rev.* 44:655–683.
3. Rojas, E. R., G. Billings, …, K. C. Huang. 2018. The outer membrane is an essential load-bearing element in Gram-negative bacteria. *Nature.* 559:617–621.
4. Raetz, C. R. H., and C. Whitfield. 2002. Lipopolysaccharide endotoxins. *Annu. Rev. Biochem.* 71:635–700.
5. De Castro, C., M. Parrilli, …, A. Molinaro. 2010. Microbe-associated molecular patterns in innate immunity. *In* Methods in Enzymology. M. Fukuda, ed Academic Press Inc, pp. 89–115.
6. Laguri, C., A. Silipo, …, J. P. Simorre. 2018. Solid State NMR Studies of Intact Lipopolysaccharide Endotoxin. *ACS Chem. Biol.* 13:2106–2113.
7. Günsel, U., and F. Hagn. 2022. Lipid Nanodiscs for High-Resolution NMR Studies of Membrane Proteins. *Chem. Rev.* 122:9395–9421.
8. Dörr, J. M., S. Scheidelaar, …, J. A. Killian. 2016. The styrene–maleic acid copolymer: a versatile tool in membrane research. *Eur. Biophys. J.* 45:3–21.
9. Laguri, C., P. Sperandeo, …, J. P. Simorre. 2017. Interaction of lipopolysaccharides at intermolecular sites of the periplasmic Lpt transport assembly. *Sci. Rep.* 7:9715.
10. Abbas, M., M. Maalej, …, C. Laguri. 2023. The unique three-dimensional arrangement of macrophage galactose lectin enables E. coli LipoPolySaccharides recognition through two distinct interfaces. *PNAS Nexus.* 2:pgad310.
11. Cian, M. B., N. P. Giordano, …, Z. D. Dalebroux. 2020. Separation of the cell envelope for gram-negative bacteria into inner and outer membrane fractions with technical adjustments for acinetobacter baumannii. *J. Vis. Exp.* 2020:1–8.
12. Vallet, A., A. Favier, …, P. Schanda. 2020. ssNMRlib: a comprehensive library and tool box for acquisition of solid-state nuclear magnetic resonance experiments on Bruker spectrometers. *Magn. Reson.* 1:331–345.
13. Buchholz, K. R., M. Reichelt, …, J. G. Quinn. 2024. Potent activity of polymyxin B is associated with long-lived super-stoichiometric accumulation mediated by weak-affinity binding to lipid A. *Nat. Commun.* 15:4733.
14. Nečas, D., and P. Klapetek. 2012. Gwyddion: An open-source software for SPM data analysis. *Cent. Eur. J. Phys.* 10:181–188.
15. Chen, S. W. W., and J. L. Pellequer. 2011. DeStripe: Frequency-based algorithm for removing stripe noises from AFM images. *BMC Struct. Biol.* 11:7.
16. Chen, S. W. W., A. S. Banneville, …, J. L. Pellequer. 2020. Nanoscale surface structures of DNA bound to Deinococcus radiodurans HU unveiled by atomic force microscopy. *Nanoscale.* 12:22628–22638.
17. Chen, S. W. W., J. M. Teulon, …, J. L. Pellequer. 2016. Atomic force microscope, molecular imaging, and analysis. *J. Mol. Recogn.* 29:51–55.
18. Maalej, M., R. E. Forgione, …, A. Silipo. 2019. Human Macrophage Galactose-Type Lectin (MGL) Recognizes the Outer Core of Escherichia coli Lipooligosaccharide. *Chembiochem.* 20:1778–1782.
19. Paracini, N., L. A. Clifton, …, J. H. Lakey. 2018. Liquid crystalline bacterial outer membranes are critical for antibiotic susceptibility. *Proc. Natl. Acad. Sci. USA.* 115:E7587–E7594.
20. Miyashita, A., S. Iyoda, …, C. Kaito. 2012. Lipopolysaccharide O-antigen of enterohemorrhagic Escherichia coli O157:H7 is required for killing both insects and mammals. *FEMS Microbiol. Lett.* 333:59–68.
21. Michino, H., K. Araki, …, H. Yanagawa. 1999. Massive outbreak of Escherichia coli O157:H7 infection in schoolchildren in Sakai City, Japan, associated with consumption of white radish sprouts. *Am. J. Epidemiol.* 150:787–796.
22. Kim, S., J. Zhang, …, E. E. Bolton. 2024. Glycoscience data content in the NCBI Glycans and PubChem. *Anal. Bioanal. Chem.* 417:865–878.
23. Renault, M., R. Tommassen-Van Boxtel, …, M. Baldus. 2012. Cellular solid-state nuclear magnetic resonance spectroscopy. *Proc. Natl. Acad. Sci. USA.* 109:4863–4868.
24. Wang, W., H. J. Sass, …, S. Grzesiek. 2008. Structure and Dynamics of ^{13} C, ^{15} N-Labeled Lipopolysaccharides in a Membrane Mimetic. *Angew. Chem. Int. Ed.* 47:9870–9874.
25. Doyle, M. T., J. R. Jimah, …, H. D. Bernstein. 2022. Cryo-EM structures reveal multiple stages of bacterial outer membrane protein folding. *Cell.* 185:1143–1156.e13.
26. Schanda, P., S. Triboulet, …, J. P. Simorre. 2014. Atomic model of a cell-wall cross-linking enzyme in complex with an intact bacterial peptidoglycan. *J. Am. Chem. Soc.* 136:17852–17860.
27. Lends, A., G. Lamon, …, A. Loquet. 2025. Molecular Distinction of Cell Wall and Capsular Polysaccharides in Encapsulated Pathogens by In Situ Magic-Angle Spinning NMR Techniques. *J. Am. Chem. Soc.* 147:6813–6824.
28. Amor, K., D. E. Heinrichs, …, C. Whitfield. 2000. Distribution of core oligosaccharide types in lipopolysaccharides from Escherichia coli. *Infect. Immun.* 68:1116–1124.

29. Müller-Loennies, S., B. Lindner, and H. Brade. 2002. Structural analysis of deacylated lipopolysaccharide of *Escherichia coli* strains 2513 (R4 core-type) and F653 (R3 core-type). *Eur. J. Biochem.* 269:5982–5991.

30. Johnson, C. L., H. Ridley, …, J. H. Lakey. 2014. The antibacterial toxin colicin N binds to the inner core of lipopolysaccharide and close to its translocator protein. *Mol. Microbiol.* 92:440–452.

31. Marchetti, R., L. Malinovska, …, A. Silipo. 2012. Burkholderia cenocepacia lectin A binding to heptoses from the bacterial lipopolysaccharide. *Glycobiology.* 22:1387–1398.

32. Schmidt, V., and J. N. Sturgis. 2018. Modifying styrene-maleic acid copolymer for studying lipid nanodiscs. *Biochim. Biophys. Acta. Biomembr.* 1860:777–783.

33. Wang, K. F., R. Nagarajan, …, T. A. Camesano. 2011. Characterization of Supported Lipid Bilayer Disruption By Chrysophsin-3 Using QCM-D. *J. Phys. Chem. B.* 115:15228–15235.

34. Richter, R. P., R. Bérat, and A. R. Brisson. 2006. Formation of Solid-Supported Lipid Bilayers: An Integrated View. *Langmuir.* 22:3497–3505.

35. Sauerbrey, G. 1959. Verwendung von Schwingquarzen zur Wägung dünner Schichten und zur Mikrowägung. *Z. Phys.* 155:206–222.

36. Hianik, T., M. Haburcák, …, A. Hermetter. 1998. Compressibility and density of lipid bilayers composed of polyunsaturated phospholipids and cholesterol. *Colloids Surf. A Physicochem. Eng. Asp.* 139:189–197.

37. Reviakine, I., D. Johannsmann, and R. P. Richter. 2011. Hearing What You Cannot See and Visualizing What You Hear: Interpreting Quartz Crystal Microbalance Data from Solvated Interfaces. *Anal. Chem.* 83:8838–8848.

38. Ledger, E. V. K., A. Sabnis, and A. M. Edwards. 2022. Polymyxin and lipopeptide antibiotics: membrane-targeting drugs of last resort. *Microbiology (N. Y.).* 168:001136.

39. Sabnis, A., K. L. H. Hagart, …, A. M. Edwards. 2021. Colistin kills bacteria by targeting lipopolysaccharide in the cytoplasmic membrane. *eLife.* 10:e65836.

40. Kern, T., S. Hediger, …, J. P. Simorre. 2008. Toward the characterization of peptidoglycan structure and protein-peptidoglycan interactions by solid-state NMR spectroscopy. *J. Am. Chem. Soc.* 130:5618–5619.

41. Noh, I., Z. Guo, …, L. Zhang. 2023. Cellular Nanodiscs Made from Bacterial Outer Membrane as a Platform for Antibacterial Vaccination. *ACS Nano.* 17:1120–1127.